SIMULTANEOUS WALL PRESSURE - PIV MEASUREMENTS IN A SHOCK WAVE / TURBULENT BOUNDARY LAYER INTERACTION

Sebastien Piponniau
Institut PPRIME, UPR 3346
CEAT, 43, rue de l'aerodrome
86000 Poitiers, France
sebastien.piponniau@ec-lyon.fr

Erwan Collin
Institut PPRIME, UPR 3346
CEAT, 43, rue de l'aerodrome
86000 Poitiers, France
erwan.collin@lea.ensma.fr

Pierre Dupont
IUSTI, UMR CNRS 6595
5, Rue Enrico Fermi
13453 Marseille Cedex 13, France
pierre.dupont@polytech.univ-mrs.fr

Jean-francois Debieve
IUSTI, UMR CNRS 6595
5, Rue Enrico Fermi
13453 Marseille Cedex 13, France
debieve@polytech.univ-mrs.fr

ABSTRACT

We present here experimental results in a shock wave / turbulent boundary layer interaction at Mach number of 2.3 impinged by an oblique shock wave, with a deflection angle of 9.5°, as installed in the supersonic wind tunnel of the IUSTI laboratory, France. For such a shock intensity, strong unsteadiness are developing inside the separated zone involving very low frequencies associated with reflected shock motions, together with a mean three dimensional organization of the flow.

The present work consists in simultaneous PIV velocity fields and unsteady wall pressure measurements. The wall pressure and PIV measurements were used to characterize the pressure distribution at the wall in an axial direction, and the flow field associated. These results give access for the first time to the spatial-time correlation between wall pressure and velocity in a shock wave turbulent boundary layer interaction and show the feasibility of such coupling techniques in compressible flows. Linear Stochastic Estimation (LSE) coupled with Proper Orthogonal Decomposition (POD) has been applied to these measurements, and first results are presented here show the ability of these techniques to predict the unsteady breathing of the recirculating bubble.

INTRODUCTION

Shock waves / boundary layer interactions occur in various aeronautical configurations, as inlets of supersonic aircrafts or in over-expanded nozzles. Different kind of such interactions can be found. An important family of shock wave / boundary layer interactions is the case when the shock is strong enough to make the boundary layer separate and reattach downstream. A strong unsteadiness is then observed, both for the separated bubble flow as for the separation shock wave, with typical frequencies at least two order of magnitude lower than the energetically frequencies of the incoming boundary layer. This low frequency behavior can lead to important pressure and thermal loads on the structure.

The main goals of the active research on shock wave boundary layer interactions are today to explain the origin of the low frequency unsteadiness of the separation shock. Two main approaches have been considered to explain this low frequency behavior : the first one is to consider the intermittent passing of very large structures present in the incoming flow through the shock (Brusniak and Dolling, 1994; Ganapathisubramani et al., 2007) leading to the observed low frequencies unsteadiness. A second approach relates the low frequency shock motions to the dynamic of the low frequency breathing of the separated bubble, located just downstream (Piponniau et al., 2009; Wu and Martin, 2008). At the light of recent work (e.g. Souverein et al., 2009), this second hypothesis is becoming more and more plausible. A simple model has been developed, and relates the low frequency unsteadiness of the recirculating bubble to the mass flux which is entrained by the shear layer in the second part of the bubble. Nevertheless a better understanding of the coupling between this shock and the dynamic of the mixing layer developing over the separated bubble is still needed to clarify the mechanisms leading to the low frequency unsteadiness of such interactions. Another point is to clarify the origin of the large-scale spanwise modulations found experimentally and numerically within the separation bubble, and their link with the unsteadiness of the interaction.

The present study deals with synchronous measurements of unsteady wall pressure and PIV measurements in a shock wave / boundary layer interaction at Mach number 2.3 with a deflection angle of 9.5°. Using stochastic methods, coupled pressure-velocity measurements are post-processed in order to build time-resolved estimated velocity fields. These fields are then used to provide information on spatio-temporal features in the flow.
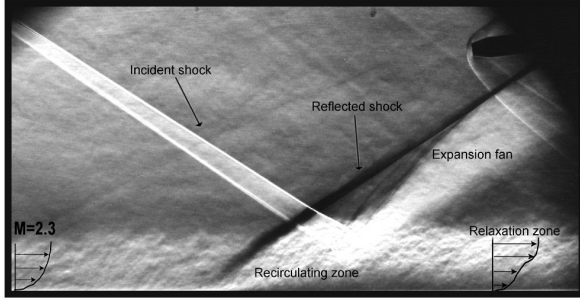
Figure 1.   Schlieren visualization of the interaction, $\theta = 9.5°$

1   EXPERIMENTAL SETUP

Experiments were carried out in the hypo-turbulent supersonic wind tunnel of the IUSTI laboratory, located in Marseille, France. This facility has been already used for shock wave / boundary layer interactions study, and therefore the flow is well documented, both for the global mean and turbulent organization of the flow as for the unsteadiness and time scales of this interaction (Dupont et al., 2006, 2008; Dussauge et al., 2006).

Table 1.   Aerodynamic parameters of the flow upstream of the interaction.

M	Re_{δ_2}	U_∞	δ_0
2.28	$5.07 \cdot 10^3$	$550\,ms^{-1}$	$11\,mm$

This wind tunnel is a continuous facility with a closed-loop circuit. The incident shock wave is generated by a sharped leading edge fixed on the ceiling of the test section, with an inclination θ, fixed at $\theta = 9.5°$ for these present experiments. The nominal conditions of the interaction are summarized in table 1. A Schlieren of the interaction is presented in figure 1.

The rectangular test section is $170\,mm$ wide by $120\,mm$ height. The origin of the longitudinal coordinate X was fixed at the mean position X_0 of the unsteady reflected shock on the axis of the wind tunnel. This position was derived from unsteady wall pressure measurements. It was normalized by the length of interaction L defined as the distance between X_0 and the extrapolation down to the wall of the incident shock. The length of the interaction was of $L = 65.5\,mm$. The transverse length Z is normalized by L, and the altitude coordinate y by the thickness of the incoming boundary layer δ_0. Normalized coordinates are then defined as:

$$\begin{cases} X^* = X/L \\ Y^* = Y/\delta_0 \end{cases} \tag{1}$$

PIV measurements

Velocity fields were obtained with Particle Image Velocimetry (PIV) measurements. The PIV investigation was made using a *Dantec Dynamics* system. Set of measurements were made in a vertical plane, along the longitudinal axis of the wind tunnel, in a set-up similar to the experimental configuration described in previous papers, see for example Dupont et al. (2008). Incense smoke was used as seeding particles. The particles were injected from the wall upstream of the sonic section of the wind tunnel. As the wind tunnel stagnation pressure was less than atmospheric, the particles were naturally entrained into the flow. The diameter of the particle is estimated to be of $0.5\mu m$, with a frequency response of about $200 kHz$.

The light sheets for the vertical PIV measurements were generated by a double pulse Nd:Yag Laser New Wave Solo III, which delivered $50 mJ$ per pulse, and separated in time by $1\mu s$. The particle images were recorded by FlowSense cameras (1600×1200 pixels), using a Nikon $60 mm f/2.8$ macro lens. The field of view is of approximately $80 mm$ wide by $60 mm$ height, but just a field of view of $80 \times 20 mm$ will be used for post-treatment, since the external flow is not seeded.

In order to have a good statistical convergence, and for further post-treatments based on conditional analysis or stochastic methods, sets of 10000 PIV vectors fields were acquired with an acquisition rate of 15Hz. The inter-correlation was carried out recursively from a cell of size 128×64 to a final cell size of 32 pixels horizontally by 16 pixels vertically, with a Gaussian weighting window applied to the interrogation cell. Therefore, the final effective cell size is 16×8 pixels; this led to a PIV resolution of $1 \times 0.5 mm^2$. An overlap of 50% between cells provided a field of 80×39 vectors.

Unsteady wall pressure measurements

The aim of these experiments is to make simultaneous unsteady wall pressure measurements in the exact location of PIV measurements, using Kulite XCQ-062 sensors. It is well known that these kinds of sensors are very sensitive, due to the thin and fragile membrane, directly exposed to the flow. In our experiments, the Kulite transducers are going to be exposed directly to the seeding particles, made of oil. During experiments, these particles settle on the floor of the wind tunnel, leading to a strong clogging. In order to protect the sensors, it has been chosen to place them behind a cavity. The dimension of the cavity was chosen to be very small in order to minimize the damping and phase shift of the measured signal against the actual signal on the wall surface.

Five Kulite sensors were used, located on the axis of the wind tunnel in the interaction region. The positions of these sensors are given in table 2. Acquisition of the pressure signals is performed synchronously during the whole experiment, using a *ETEP* data acquisition system, at a sampling frequency of 400kHz, and digitally filtered at 100kHz via a *sigma/delta* filter before storage. Also, to avoid noise in the highest frequencies, a low-pass filter is performed on the pressure signals (5th-order Butterworth filter for $f > 20 kHz$).

For the synchronization of the PIV and time-resolved pressure measurement, the exposure signal of the camera of each frame was recorded with the *ETEP* system used for the pressure transducer signals, leading to a maximum time dis-

Table 2. Location of pressure sensors at the wall

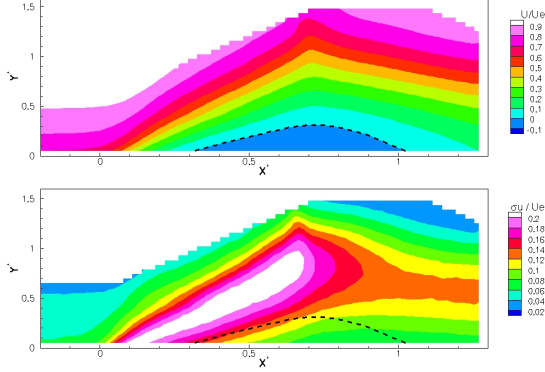| Kulite sensor	#1	#2	#3	#4	#5
X^*	0	0.29	0.49	0.74	1

Figure 2. Contours of average longitudinal velocity and standard deviation of longitudinal velocity fluctuations (dashed line corresponds to the boundary of the recirculation bubble

crepancy of $10\mu s$ due to the recording rate.

The aim of these experiments is to make simultaneous unsteady wall pressure measurements in the exact location of PIV measurements, using Kulite sensors. It is well known that these kind of sensors are very sensitive, due to the thin and fragile membrane, directly exposed to the flow. In our experiments, the Kulite transducers are going to be exposed directly to the seeding particles, made of oil. During experiments, this particles settle on the floor of the wind tunnel, leading to a strong clogging. In order to protect the sensors, it has been chosen to place them behind a cavity.This cavity has no significant effect on the amplitude and phase of pressure signals in the frequency range considered.

PROPER ORTHOGONAL DECOMPOSITION OF VELOCITY FIELDS

Averaged velocity contours and standard deviation are plotted in figure 2. Only the region located inside the boundary layer is considered: the signal to noise ratio is not sufficient outside this area.

A proper orthogonal decomposition (POD) is performed on the set of 10 000 instantaneous PIV fields. The POD is a useful tool for extracting large scale features and coherent structures in turbulent flows (Lumley, 1967; Aubry et al., 1988; Ukeiley et al., 2001). It consists in extracting from the flow the structure $\Phi(\mathbf{x})$ with the largest mean-square projection onto the velocity field $\mathbf{u}(\mathbf{x},t)$. The maximization problem leads to the solving of the integral problem of eigen values:

$$\int_{\mathscr{D}} R(\mathbf{x},\mathbf{x}')\,\Phi_n(\mathbf{x}')d\mathbf{x}' = \lambda_n\,\Phi_n(\mathbf{x}) \qquad (2)$$

where λ_n corresponds to the nth eigen value and represents the amount of energy contained in the spatial mode $\Phi_n(\mathbf{x})$. $R(\mathbf{x},\mathbf{x}')$ is the two-point temporal correlation tensor defined as $R(\mathbf{x},\mathbf{x}') = \langle \mathbf{u}(\mathbf{x},t)\mathbf{u}(\mathbf{x}',t)\rangle$, where $\langle \cdot \rangle$ is the ensemble average operator. The modes are sorted in the descending order: $\lambda_1 > \lambda_2 > \cdots > \lambda_{N_{POD}} > 0$.

In the context of the present study, we use a snapshot POD method (Sirovitch, 1987) to extract POD modes from the PIV dataset. In the end, the fluctuating field can be projected onto the POD orthonormal basis, composed of the eigen functions $\Phi_n(\mathbf{x})$:

$$\mathbf{u}(\mathbf{x},t) = \sum_{n=1}^{N_{POD}} a_n(t)\cdot\Phi_n(\mathbf{x}) \qquad (3)$$

where N_{POD} is the number of PIV samples. The temporal projection coefficients $a_n(t)$ contain the energy:

$$\langle a_i \cdot a_j \rangle = \delta_{ij}\lambda_i \qquad (4)$$

The POD eigen spectra for the fields acquired by PIV in the present study is plotted in figure 3. We observe a rapid decrease of $\lambda_n \sim n^{-0.9}$, which is close to $n^{-11/9}$, a value commonly observed for POD on velocity fields of turbulent flows (Knight and Sirovich, 1990). For $n > 3000$, the eigen values fall to near 0, which is consistent with the degree of freedom of the PIV fields (e.g. number of vectors in each field).
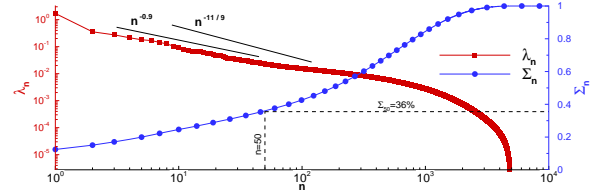

Figure 3. Eigen spectra and cumulative relative energy in the first n modes

The spatial eigen modes $\Phi_n(\mathbf{x})$ are plotted in figure 4 for $n = 1,6$. It appears that various flow features are contained in these modes, indicating that POD-filtered fields taking into account only few first modes could be sufficient to characterize large-scale features in the interaction region.
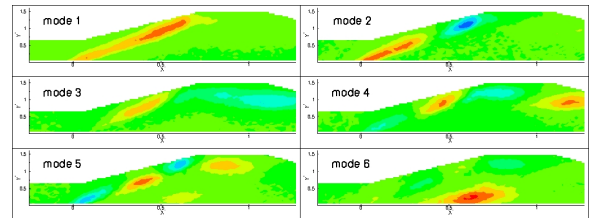

Figure 4. First 6 spatial eigen modes from the snapshot POD of the PIV fields

3

LINEAR ESTIMATION OF THE VELOCITY FIELD

The Linear Stochastic Estimation (LSE) is a method which is a generalized conditional averaging, with the use of multiple conditional parameters (Adrian, 1979; Adrian and Moin, 1988). In the present study, the LSE is to be performed on the velocity field, using the wall pressure signals as conditional parameters. The variant of the LSE which is used is the complementary method: instead of estimating the velocity itself, we estimate the temporal coefficients of POD modes. We choose the complementary method because of two important points. First, this method takes advantage that the POD is a way to separate time and space variables. Second, the complementary technique is only performed on the first N_{LSE} POD modes, and then it concerns POD-filtered data. The complementary technique focuses on large-scale and energetic features of the flow that are contained in the first N_{LSE} POD modes.

In order to prepare the linear stochastic estimation, it is important to analyze the temporal correlation functions between the pressure signals P_k and the POD temporal coefficients of the velocity fields a_n. These correlation functions are defined as:

$$R_{a_n,P_k}(dt) = \frac{\langle a_n(t) \cdot P_k(t+dt) \rangle}{\sqrt{\langle a_n^2 \rangle \cdot \langle P_k^2 \rangle}} \quad (5)$$

and are plotted in figure 5 for POD modes #1 to 6. The signs of R_{a_n,P_k} are not discussed: the signs of the POD modes have no signification. The signal of the pressure sensor #1 (located near the foot of the reflected shock) is strongly correlated with most of the POD modes, even for $dt = 0$. The whole region of interaction is then correlated with the low frequencies oscillations of the reflected shock wave, and the sensor #1 is a good indicator for these oscillations. The correlation for pressure sensors #2 to #5, while weaker than for sensor #1, are non negligible, especially for non-zero time delays. These sensors contain information of convective/propagative features of the flow: fluctuations in the mixing layer (e.g. modes 5), vortex shedding (e.g. mode 4). The POD mode 6, which is relative to the intensity of the recirculating bubble, is strongly correlated with the pressure sensor #4: this sensor is located in the middle of the bubble.

To optimize the meaning of the conditional parameters, the temporal POD coefficients are estimated using the pressure signals for for time delays which correspond to the maximum of correlation. The formalism of the LSE is:

$$\tilde{a}_n(t) = \sum_{k=1}^{N_{KUL}} A_{k,n} \cdot P_k(t + \Delta t_{k,n}) \quad (6)$$

where $\tilde{a}_n(t)$ is the estimated temporal coefficient for the nth POD mode at time t, N_{KUL} is the number of pressure sensors, $A_{k,n}$ are the LSE coefficients, and $\Delta t_{k,n}$ the time delays which correspond to the maximum of $\left| R_{a_n,P_k}(dt) \right|$.

The fact that the time delay depends on both n and k multiplies the amount of information used to build the estimations. If no time delay is used, the number of POD modes

which could be estimated would not exceed the number of conditional parameters (Perret, 2004). Here, with the multi time delay approach, it is expected that the degree of freedom of the estimated field will not be limited by the number of sensors.
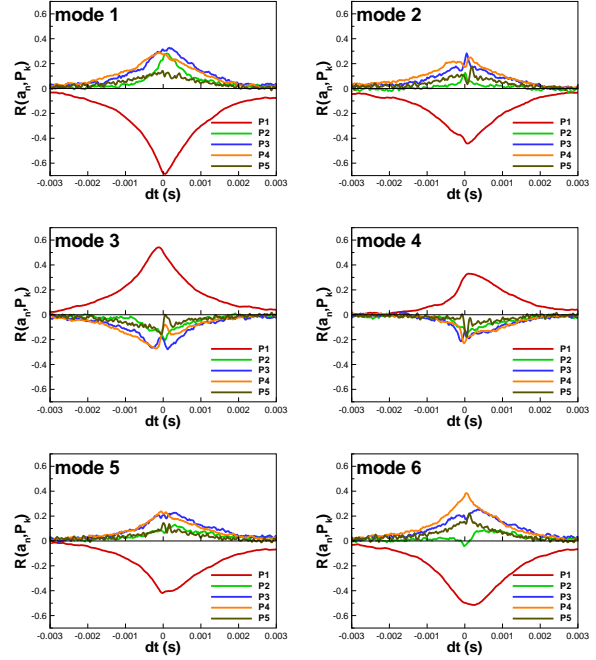

Figure 5. Correlation functions $R_{a_n,P_k}(dt)$ for the first 6 POD modes

The LSE coefficients are obtained solving the least-square problem:

$$\langle a_n(t)P_{k'}(t + \Delta t_{k',n}) \rangle \quad (7)$$
$$= \sum_{k=1}^{N_{KUL}} A_{k,n} \langle P_k(t + \Delta t_{k,n}) \cdot P_{k'}(t + \Delta t_{k',n}) \rangle$$

Once the $A_{k,n}$ are known, we can produce a set of $\tilde{a}_n$ and build an estimated velocity field which is a partial POD reconstruction based on the N_{LSE} first modes:

$$\tilde{\mathbf{u}}(\mathbf{x},t) = \sum_{n=1}^{N_{LSE}} \tilde{a}_n(t) \cdot \Phi_n(\mathbf{x}) \quad (8)$$

The POD-LSE complementary method is performed in the present study using the first $N_{LSE} = 50$ POD modes, which represent 36% of the total energy. Such a number of POD modes is enough to reproduce the global shape of the interaction and large-scale structures in the separated shear layers.

Firstly, the LSE is performed for times that correspond to original PIV data, in order to evaluate the relevance of the estimation. Two examples of estimated velocity contours are given in figure 6. The loss of information is progressive between the original complete field, the partial reconstruction

using only 50 POD modes, and the final estimated field reconstructed with the estimated first 50 POD coefficients. However, the global shape of the recirculating bubble, the location of the separation point and large-scale distortion of shear layers are well reproduced by the complementary technique.
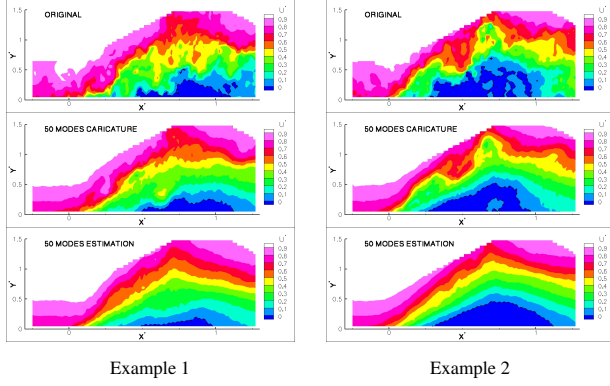

Example 1   Example 2

Figure 6.   Comparisons between original fields, 50-modes caricatures and estimated fields for the corresponding times.

It is important also to check that the degree of freedom of the estimated fields are not constrained by the fact that only 5 pressure signals are used, whereas 50 POD modes are estimated. This can be done using an other POD decomposition on a set of estimated velocity fields. Figure 7 shows the eigen spectra for this POD. It is clear that the degree of freedom of the estimated fields corresponds to the number of estimated POD modes. The multi-time delays procedure allowed to take into account enough information in the conditional signals without major redundancy. One can also notice on figure 7 that the decay rate is $\lambda_n \sim n^{-2}$. This is due to the quadratic relationship between the dynamic pressure and the velocity: the last POD is performed on velocity fields estimated from pressure measurements.
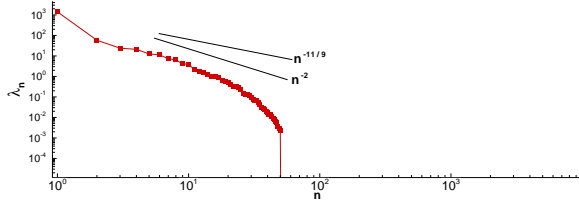

Figure 7.   Eigen spectra of the estimated velocity samples

ANALYSIS OF TIME-RESOLVED ESTIMATED VELOCITY FIELDS

Since the complementary POD-LSE technique gives satisfaction for both the recirculation zone and the large-scale features of shear layers it is interesting to take advantage of the stochastic tool to produce and analyze time-resolved estimated velocity fields. Four points are selected in the flow, noted A, B, C and D. The location of these points are illustrated on the figure 8. Point A and B are located on the outer side of the separated shear layer, while points C and D are located near the wall, inside the recirculation bubble.
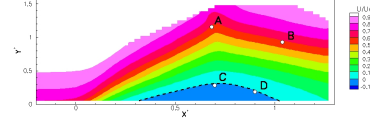

Figure 8.   Location of the points selected for cross-spectra analysis

For each of these points, an estimated signal is built with the same temporal resolution as for the pressure signals. The coherence function Γ, phase shift ϕ and phase velocity U_ϕ for points {A,B} and points {C,D} are plotted in figure 9 and 10. These results are plotted with the normalized frequency: $St_L = f.L/U_e$. The coherence function is defined as:

$$\Gamma(f) = \frac{G_{xy}^2(f)}{|G_{xx}(f)| \cdot |G_{yy}(f)|} \qquad (9)$$

where G_{xx} and G_{yy} are the power spectra for points x and y and G_{xy} is the cross-spectra between x and y. The phase velocity is defined as:

$$U_\phi = \frac{2\pi \cdot f \cdot \Delta\mathbf{x}}{-\phi \pm n\pi} \qquad (10)$$

where $\Delta\mathbf{x}$ is the spacing between the two points. The convention for the phase is that $\phi < 0$ indicates that the signal for the second point of a pair is delayed with respect to the signal for the first point. Therefore, $U_\phi > 0$ corresponds to a phase velocity in the downstream direction. For a given frequency f, ϕ and U_ϕ are to be considered only if $\Gamma(f) > 0.1$.

For the pair {A,B}, located at the outer side of the shear layer, strong coherence levels are obtained at very low frequency $St_L < 0.1$, associated with a zero phase-shift. This is related to the pulsations of the bubble. A secondary peak of coherence occurs at $St_L \sim 0.4$, associated with linear variations of ϕ. The phase velocity for this peak is $U_\phi \sim 220 ms^{-1}$. Both the frequency and the phase velocity for this peak correspond to the Kelvin-Helmholtz instability of the shear layer. A third peak is also detected at $St_L \sim 1.1$. It is associated with a constant phase of $\phi \sim \pm\pi$. Thus, the fluctuations linked with this peak are not convected. In the highest frequency range, a peak of coherence are also detected, at $St_L \sim 1.8$, associated with $U_\phi \sim 220 ms^{-1}$.

For the pair {C,D}, located inside the recirculation bubble, high coherence levels are detected at $St_L < 0.1$, with a non zero phase shift. The associated convective velocity is in the downstream direction and varies from $U_\phi \sim 55 ms^{-1}$ to $U_\phi \sim 220 ms^{-1}$ in the frequency range $0 < St_L < 0.5$. For $St_L \geq 0.6$, several significant peaks of coherence can also be observed, with linear variations of ϕ, leading to a phase velocity almost constant $U_\phi \sim 150 ms^{-1}$, in the downstream direction. Such a phase velocity has been obtained by Dupont et al. (2006) in the region $0.5 < X^* < 0.8$, from wall-pressure measurements.
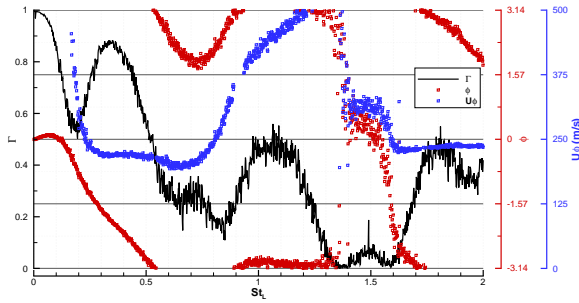
Figure 9. Coherence function, phase and phase velocity for estimated signals at points {A,B}
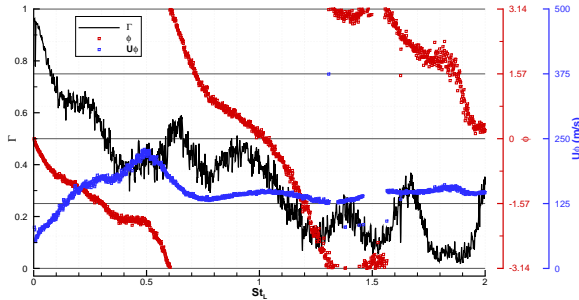

Figure 10. Coherence function, phase and phase velocity for estimated signals at points {C,D}

CONCLUSIONS

Coupled PIV and unsteady wall pressure measurements have been performed in a shock-wave / turbulent boundary layer interaction. The data have been post-processed using a complementary POD/LSE method in order to build velocity fields estimated from wall pressure signals. The complementary technique is achieved using multiple time delays in order to enhance the amount of information on which the estimation is based.

The comparison between original and estimated fields have shown that the complementary method is able to afford estimations of the shape of the separation zone, the location of the separation point and the large scale instantaneous distortions of the shear layers. The stochastic tool has been also used to produce time-resolved unsteady velocity fields. Cross-spectra of estimated velocity have been analyzed for two pairs of point location in the interaction. The time-resolved unsteady velocity fields exhibit both features linked to local instabilities (Kelvin-Helmholtz waves convected in the free shear layer) and features relative to the pulsation of the bubble at low frequency. The cross-spectra also put forward some complex interactions between points located inside the recirculation bubble. Particularly, a constant phase velocity $U_\phi \sim 140 ms^{-1}$ has been detected for a wide frequency range inside the bubble.

Interpretation of the dynamics of the estimated fields must be made very carefully: the estimated fields represent only a low-order description of a part of the flow which is correlated with wall pressure fluctuations. The results still need to be compared with unsteady two-points velocity measurements.

REFERENCES

Adrian, R. (1979). Conditional eddies in isotropic turbulence. *Physics of Fluids*, 22(11):2065–70.

Adrian, R. and Moin, P. (1988). Stochastic estimation of organized turbulent structure: homogeneous shear flow. *J. Fluid Mech.*, 190:531–559.

Aubry, N., Holmes, P., Lumley, J., and Stone, E. (1988). The dynamics of coherent structures in the wall region of a turbulent boundary layer. *J. Fluid Mech.*, 192:115–173.

Brusniak, L. and Dolling, D. S. (1994). Physics of unsteady blunt-fin-induced shock wave/turbulent boundary layer interactions. *Journal of Fluid Mechanics*, 273:375–409.

Dupont, P., Haddad, C., and Debiève, J. F. (2006). Space and time organization in a shock induced boundary layer. *Journal of Fluid Mechanics*, 559:255–277.

Dupont, P., Piponniau, S., Sidorenko, A., and Debiève, J. F. (2008). Investigation of an oblique shock reflection with separation by PIV measurements. *AIAA Journal*, 46(6).

Dussauge, J. P., Dupont, P., and Debiève, J. F. (2006). Unsteadiness in shock wave boundary layer interactions with separation. *Aerospace Science and Technology*, 10:85–91.

Ganapathisubramani, B., Clemens, N. T., and Dolling, D. S. (2007). Effects of upstream coherent structures on low-frquency motion of shock-induced turbulent separation. In *45th AIAA Aerospace Sciences Meeting and Exhibit, Reno, Nevada, 8-11 January*.

Knight, B. and Sirovich, L. (1990). Kolmogorov inertial range for inhomogeneous turbulent flows. *Phys. Review Letters*, 65(11):1356–1539.

Lumley, J. (1967). The structure of inhomogeneous turbulent flows. In Yalgom and Tatarsky, editors, *Atm. turb. and radio wave prop.*, pages 166–178. Atm. turb. and radio wave prop.

Perret, L. (2004). *Etude du couplage instationnaire calculs-expériences en écoulements turbulents*. PhD thesis, University of Poitiers.

Piponniau, S., Dussauge, J. P., Debiève, J. F., and Dupont, P. (2009). A simple model for low-frequency unsteadiness in shock-induced separation. *Journal of Fluid Mechanics*, 629:87–108.

Sirovitch, L. (1987). Turbulence and the dynamics of coherent structures. *Quarterly of Applied Mathematic*.

Souverein, L. J., Van Oudheusden, B. W., Scarano, F., and Dupont, P. (2009). Application of a dual-plane particle image velocimetry (dual-PIV) technique for the unsteadiness characterization of a shock wave turbulent boundary layer interaction. *Measurement Science and Technology*, 20(7).

Ukeiley, L., Cordier, L., Manceau, R., Delville, J., Glauser, M., and Bonnet, J. (2001). Examination of large-scale structures in a turbulent plane mixing layer. part 2. dynamical systems model. *J. Fluid Mech.*, 441:67–108.

Wu, M. and Martin, M. P. (2008). Analysis of shock motion in shockwave and turbulent boundary layer interaction using direct numerical simulation data. *Journal of Fluid Mechanics*, 594:71–83.